A method for parametric analysis of stability boundaries for nonlinear periodic vibrations of structures with contact interfaces

Article (Accepted Version)

Proceedings of ASME Turbo Expo 2018: Turbomachinery Technical Conference and Exposition
GT2018
June 11-15, 2018, Oslo, Norway

GT2018-76545

A METHOD FOR PARAMETRIC ANALYSIS OF STABILITY BOUNDARIES FOR NONLINEAR PERIODIC VIBRATIONS OF STRUCTURES WITH CONTACT INTERFACES

E.P. Petrov

University of Sussex, School of Engineering and Informatics,
Brighton BN1 9QT, United Kingdom, Email: y.petrov@sussex.ac.uk

ABSTRACT

A method for parametric analysis of the stability loss boundary has been developed for periodic regimes of nonlinear forced vibrations for a first time. The method allows parametric frequency-domain calculations of the stability loss together with the vibration amplitudes and design parameter values corresponding to the stability boundaries. The tracing algorithm is applied to obtain the trajectories of stability loss points as functions of design parameters. The parametric stability loss is formulated for cases when: (i) the design parameters characterise the properties of nonlinear contact interfaces (e.g. gap, contact stiffness, friction coefficient, etc.) and (ii) the design parameters describe linear components of the analysed structure (e.g. parameters of geometric shape, material, natural frequencies, modal damping etc.) and (iii) these parameters describe the excitation loads (e.g. their level, distribution or frequency). An approach allowing the multiparametric analysis of stability boundaries is proposed. The method uses the multiharmonic representation of the periodic forced response and aimed at the analysis of realistic gas-turbine structures comprising thousands and millions degrees of freedom. The method can be used for the effective search of isolated branches of the nonlinear solutions and examples of detection and search of the isolated branches are given: for relatively small and for large-scale finite element models. The efficiency of the method for calculation of the stability boundaries and for the search of isolated branches is demonstrated on simple systems and on a large-scale model of a turbine blade.

INTRODUCTION

Gas-turbine engine and other machinery structures are assembled structures with components interacting at contact interfaces. The interaction forces at these interfaces are nonlinear due to: unilateral contacts, closing and opening gaps, friction forces, variable contact areas, cubic nonlinearities due to Hertzian contacts, etc.

In majority of cases the steady-state periodic forced response is of major interest and the analysis of periodic vibration can be efficiently performed in frequency domain for realistic models of structures which customarily contain millions degrees of freedom (DOFs) (see e.g. Refs.[1]-[6]). The stability of the found nonlinear periodic vibration regimes is one of the most important characteristics which allows to differentiate: (i) unstable vibrations – which are not practically achievable in usual operating conditions and (ii) stable vibration regimes – those that can be realised and maintained.

The significant developments of methods for the stability analysis in frequency domain have been done relatively recently for systems with rather restricted number of degrees of freedom (e.g. see Refs. [7]-[11]) and for large-scale finite elements models (Ref.[12]). These methods allow the determination of the stability factors for any found periodic vibration regime. In Ref.[13] the method for analysis of sensitivity of the stability factors to contact interface parameters and design parameters of linear components of a structure was developed, which provide the useful information about how the small variations of design parameters can affect the stability of the vibrations.

In the proposed paper, the problem of calculation of the boundaries of the dynamic stability is formulated and solved for a first time. The amplitudes, vibration frequencies and design parameter values corresponding to the points where the vibration regime stability property switches between stable and unstable are calculated when one or a selected set of design parameters vary in a wide range of possible values. The multiharmonic

representation of the periodic motion is used and the method developed can analyse realistic high-fidelity models of structural components and contact interfaces.

The frequency-domain equations are formulated for the determination of vibration amplitude and design or excitation parameters at the stability loss. The condition of equality to zero the maximum real part selected from the set of calculated in frequency domain Floquet exponents is accepted here as the indicator of the stability loss.

The solution of the stability loss boundary equation is performed by Newton-Raphson method with continuation. The Jacobian and other derivatives of the equation solved are derived analytically, including derivatives of the maximum real Floquet exponent with respect to multiharmonic vibration amplitudes, frequency and design parameters. The considered here cases include the cases when the design parameters are: (i) contact interface parameters and (ii) the parameters of linear components of an assembled structure. The procedure of continuation is proposed to find the dependency of the stability boundary on the variation of the multitude of design parameters.

In the addition to the stability boundary analysis the method developed has demonstrated its high efficiency in search for the isolated solution branches, i.e. closed loop solution trajectories which are not connected to the major solution branch. This problem did not have a general solution so far, and the research in this area is still in a germinal state, although a few interesting papers considering systems with one or two DOFs should be mentioned here (see Refs.[14]-[17]).

The method has been implemented in a computer code and its efficiency and accuracy are demonstrated on a set of numerical examples: from a simple 1 DOF nonlinear oscillator to finite element models comprising 160,000 DOFs. It is shown that the method calculates the trajectories of stability loss for all models considered and for different nonlinearities. For a first time, the isolated regimes have been found for structures with large number of DOFs. The isolated branches are found here for: (i) cubic and (ii) gap nonlinearities. The existence of isolated branches and scenarios of 'a jump' from isolated branch to the major solution branch are confirmed by time integration of nonlinear equation of motion. The possibility of a structure with gap nonlinearity to lose its stability by three possible scenarios: (i) by period doubling; (ii) by transition to quasi-periodic vibration and by (iii) stability loss without period change is demonstrated.

STABILITY BOUNDARY PROBLEM FORMULATION

The equation of motion for the forced vibrations of a structure with nonlinear interactions at joints can be written in the form:

$$\boldsymbol{K}\boldsymbol{x} + \boldsymbol{C}\dot{\boldsymbol{x}} + \boldsymbol{M}\ddot{\boldsymbol{x}} + \boldsymbol{f}(\boldsymbol{x}, \dot{\boldsymbol{x}}) = \boldsymbol{p}(t) \qquad (1)$$

where $\boldsymbol{x}(t)$ is a vector of displacements for all degrees of freedom in the structure considered; $\boldsymbol{K}$, $\boldsymbol{C}$ and $\boldsymbol{M}$ are structural stiffness, damping and mass matrices of finite element (FE) model of a structure and $\boldsymbol{p}(t)$ is a vector of excitation forces; $\boldsymbol{f}(\boldsymbol{x}, \dot{\boldsymbol{x}})$ is a vector of nonlinear contact interface forces which, for a case considered here, can be explicitly dependent on displacements, $\boldsymbol{x}$ and velocities, $\dot{\boldsymbol{x}}$ of the structural components. The contact forces occur in gas-turbine structures at the blade root joints of bladed discs, at contact surfaces of underplatform or tip dampers, at contact surfaces of adjacent interlock shrouds and at rubbing contacts between rotor and casing. The causes of nonlinear behaviour are usually friction forces, unilateral interaction at the pairing contact surfaces, gaps, varying contact stiffness properties, as in the case of Hertzian contacts, etc. A case of periodic excitation forces is considered, $\boldsymbol{p}(t) = \boldsymbol{p}\left(t + 2\pi/\omega\right)$, where ω is the principal excitation frequency.

For any solution, $\boldsymbol{x}^*$, its stability can be determined by considering a perturbed motion $\boldsymbol{x} = \boldsymbol{x}^* + e^{\lambda t}\boldsymbol{s}(t)$ and considering an eigenproblem obtained by linearization of Eq.(1) (see Ref.[12]):

$$\boldsymbol{M}\left(\lambda^2\boldsymbol{s} + 2\lambda\dot{\boldsymbol{s}} + \ddot{\boldsymbol{s}}\right) + \left[\boldsymbol{C} + \frac{\partial \boldsymbol{f}}{\partial \dot{\boldsymbol{x}}}\right]\left(\lambda\boldsymbol{s} + \dot{\boldsymbol{s}}\right) + \left[\boldsymbol{K} + \frac{\partial \boldsymbol{f}}{\partial \boldsymbol{x}}\right]\boldsymbol{s} = \boldsymbol{0} \qquad (2)$$

The solution of this eigenproblem provides $2N$ eigenvalues $\left\{\lambda_j\right\}_1^{2N}$, where N is the total number of DOFs. The eigenvalues can be real or complex numbers, with the complex eigenvalues forming complex-conjugated pairs. The eigenvalue with the maximum real part defines the stability of the found solution: if $\lambda_{\mathrm{Re}}^{\max} = \max\limits_{j \in 1..2N} \mathrm{Re}\left(\lambda_j\right) > 0$, then the found motion is unstable.

A gas-turbine structure, as any other machinery structure, has usually a set of parameters which can be changed intentionally or that are uncertain and it is important to know how these parameters affect the stability properties of the nonlinear vibration regimes. For our analysis it is convenient to collect these parameters in three groups: (i) parameters which describe linear components of the analysed assembled structure, $\boldsymbol{b}^l$, such as natural frequencies, modal damping factors, material properties, parameters describing geometric shapes, etc., (ii) parameters which describe the excitation loads, $\boldsymbol{b}^p$, such as the excitation frequencies, loading levels and parameters characterising distribution of the loads over a structure, and (iii) parameters of contact interfaces, $\boldsymbol{b}^f$, such as contact stiffness, gap, friction coefficient values; level of static preloading at contact interfaces, etc. Choosing from these parameters the parameters which represent interest and then combining these parameters in a single vector we have:

$$\underset{n_p \times 1}{\boldsymbol{b}} = \left\{\boldsymbol{b}^l, \boldsymbol{b}^p, \boldsymbol{b}^f\right\}^T, \qquad (3)$$

where n_p is the total number of parameters considered in the analysis. Now, taking into account that $\lambda_{\mathrm{Re}}^{\max}$ is dependent on these parameters and the stability boundary is described by the condition: $\lambda_{\mathrm{Re}}^{\max} = 0$, we can write the equation describing the stability boundary as an implicit function of design parameters:

$$\lambda_{\mathrm{Re}}^{\max}\left(\boldsymbol{x}^*\left(\boldsymbol{b}\right), \boldsymbol{b}\right) = 0 \qquad (4)$$

When each of these parameters is considered as an independent parameter, the general form of the stability boundaries given by Eq.(4) gives an equation of the stability boundary as hyper-surface in n_p -dimensional space, e.g. for two parameters it gives an equation of a line, for three parameters it gives an equation of surface, etc. Often a significant number of design parameters are interdependent, for example they can be described as a function of a rotational speed or temperature and the variation of these design parameters can be described parametrically: $\boldsymbol{b} = \boldsymbol{b}(\tau)$, where τ is the auxiliary parameter introduced for the parameter variation description. If, for example, we consider the first of the parameters as independent and the rest are coupled by the parametric interdependence, the stability equation can be then written in the form:

$$\lambda_{\mathrm{Re}}^{\max}\left(\boldsymbol{x}^*\left(\boldsymbol{b}\right), b_1, \boldsymbol{b}_{2..n_p}(\tau)\right) = 0 \qquad (5)$$

METHOD FOR STABILITY BOUNDARY ANALYSIS

Multiharmonic equations of the stability boundary

In order to find the parametric description of the stability boundary we have to find solution, $\boldsymbol{x}^*$, and parameters, $\boldsymbol{b}$, satisfying Eqs.(1), (2) and (5). We consider in this paper stability of periodic regimes, therefore, the equation of motion given by Eq.(1) and the stability equation, Eq. (2), are formulated in the frequency-domain using multiharmonic representation of the displacements and the nonlinear forces.

$$\boldsymbol{x}(t) = \boldsymbol{H}_x^T \boldsymbol{X}\ ;\ \boldsymbol{p}(t) = \boldsymbol{H}_x^T \boldsymbol{P}\ ;\ \boldsymbol{f}(\boldsymbol{x}, \dot{\boldsymbol{x}}) = \boldsymbol{H}_x^T \boldsymbol{F}\ ;\ \boldsymbol{s}(t) = \boldsymbol{H}_S^T \boldsymbol{S} \quad (6)$$

where $\boldsymbol{X} = \left\{\boldsymbol{X}_0, \boldsymbol{X}_1^c, ..., \boldsymbol{X}_{n_x}^s\right\}^T$; $\boldsymbol{P} = \left\{\boldsymbol{P}_0, \boldsymbol{P}_1^c, ..., \boldsymbol{P}_n^s\right\}^T$; $\boldsymbol{F} = \left\{\boldsymbol{F}_0, \boldsymbol{F}_1^c, ..., \boldsymbol{F}_n^s\right\}^T$ and $\boldsymbol{S} = \left\{\boldsymbol{S}_0, \boldsymbol{S}_1^c, ..., \boldsymbol{S}_{n_S}^s\right\}^T$ are vectors of harmonic coefficients for displacements, excitation forces, nonlinear forces and for the periodic part of the perturbed motion, $\boldsymbol{s}(t)$, in the stability equation respectively. The matrices used here for the time domain expansion can be written, using Kronecker's multiplication formalism, in the form: $\boldsymbol{H}_\gamma = \left\{1, \cos\tilde{\omega}_1^\gamma t, ..., \sin\tilde{\omega}_{n_\gamma}^\gamma t\right\}^T \otimes \boldsymbol{I}$, where $\gamma = x, s$, $\tilde{\omega}_j^\gamma = k_j^\gamma \omega$ and ω is the principal frequency of the periodic motion. It should be noticed that the total number of harmonics, n_γ, and the harmonic numbers, k_j^γ, kept in the multiharmonic equation of motion and in the multiharmonic stability equation can be different, their choice is determined by the accuracy required for the analysis of nonlinear response and for the solution of the stability eigenproblem.

Moreover, since the methodology developed here is aimed at the analysis of high-fidelity models of realistic complex machinery structures which can contain millions degrees of freedom, to reduce the computation time the highly-accurate model reduction method developed in Ref.[3] is used. The method reduces the size of nonlinear multiharmonic equation of motion to the number of multiharmonic coefficients only for degrees of freedom where the nonlinear contact forces can occur practically without loss of accuracy. The multiharmonic equation of motion is obtained in the form:

$$\boldsymbol{R} = \boldsymbol{X}^n - \boldsymbol{X}^l\left(\omega, \boldsymbol{b}^l, \boldsymbol{b}^p\right) + \tilde{\boldsymbol{A}}\left(\omega, \boldsymbol{b}^l\right)\boldsymbol{F}\left(\boldsymbol{X}^n, \boldsymbol{b}^c\right) \qquad (7)$$

where $\boldsymbol{X}^n$ is vector of multiharmonic coefficients for nonlinear degrees of freedom - this vector has to be calculated, $\boldsymbol{X}^l\left(\omega, \boldsymbol{b}^l, \boldsymbol{b}^p\right)$ is vector of multiharmonic coefficients calculated in the absence of the nonlinear contacts which is dependent on the parameters of the linear components of the structure, $\boldsymbol{b}^l$, and on the excitation loading parameters, $\boldsymbol{b}^p$. The multiharmonic forced response function matrix (FRF), $\tilde{\boldsymbol{A}}$, is formed from complex FRF matrices calculated for each harmonic separately:

$$\tilde{\boldsymbol{A}} = diag\left(\boldsymbol{A}(0), \begin{bmatrix} \boldsymbol{A}_{\mathrm{Re}}^{(1)} & \boldsymbol{A}_{\mathrm{Im}}^{(1)} \\ -\boldsymbol{A}_{\mathrm{Im}}^{(1)} & \boldsymbol{A}_{\mathrm{Re}}^{(1)} \end{bmatrix}, .., \begin{bmatrix} \boldsymbol{A}_{\mathrm{Re}}^{(n_x)} & \boldsymbol{A}_{\mathrm{Im}}^{(n_x)} \\ -\boldsymbol{A}_{\mathrm{Im}}^{(n_x)} & \boldsymbol{A}_{\mathrm{Re}}^{(n_x)} \end{bmatrix}\right) \qquad (8)$$

$\boldsymbol{A}_{\mathrm{Re}}^{(j)} = \mathrm{Re}\left(\boldsymbol{A}\left(\tilde{\omega}_j^x\right)\right)$ and $\boldsymbol{A}_{\mathrm{Im}}^{(j)} = \mathrm{Im}\left(\boldsymbol{A}\left(\tilde{\omega}_j^x\right)\right)$. The FRF matrices are generated using the modal properties and reference compliance matrices as proposed in Ref.[3], which provides high accuracy required for the analysis of the dynamic contact interaction problems.

For the case considered in this paper we assume that the nonlinear forces can be explicit functions of displacement and velocities. The stability eigenproblem formulation in the frequency domain can be obtained for the case of reduced modelling in the stability analysis in the following form (see Ref. [12]):

$$\left[\lambda^2 \boldsymbol{I} + \lambda \boldsymbol{B}_1 + \boldsymbol{B}_0\right]\boldsymbol{S} = \boldsymbol{0} \qquad (9)$$

where $\boldsymbol{I}$ is identity matrix and the other matrices have the form:

$$\boldsymbol{B}_0 = \tilde{\boldsymbol{\Omega}}^2 + \tilde{\boldsymbol{C}}\boldsymbol{E}_1 - \boldsymbol{E}_2 + \tilde{\boldsymbol{\Phi}}^T \hat{\boldsymbol{K}} \tilde{\boldsymbol{\Phi}}\ ;\ \boldsymbol{B}_1 = 2\boldsymbol{E}_1 + \tilde{\boldsymbol{C}} + \tilde{\boldsymbol{\Phi}}^T \hat{\boldsymbol{C}} \tilde{\boldsymbol{\Phi}} \qquad (10)$$

where $\tilde{\boldsymbol{\Omega}} = diag\left(\boldsymbol{\Omega}, \boldsymbol{\Omega}, ,..., \boldsymbol{\Omega}\right)$ is a matrix combined from matrices of natural frequencies: $\boldsymbol{\Omega} = diag\left(\omega_1, \omega_2, ..., \omega_m\right)$; $\tilde{\boldsymbol{\Phi}} = diag\left(\boldsymbol{\Phi}, \boldsymbol{\Phi}, ...\boldsymbol{\Phi}\right)$; $\boldsymbol{\Phi}(N^n \times m)$ is a matrix of mass-normalised mode shapes of a linear structure calculated for a structure with the absence of the contact interactions; N^n is the number of nonlinear DOFs, and m is the number of mode shapes used for the model reduction. The matrices corresponding to the nonlinear forces are indicated here by a cap '$\wedge$' above the symbol and are defined as:

$$\hat{\boldsymbol{K}} = \frac{\omega}{\pi}\int_0^{2\pi/\omega} \boldsymbol{H}_S^*\left(\frac{\partial \boldsymbol{f}}{\partial \boldsymbol{x}}\boldsymbol{H}_S^T + \frac{\partial \boldsymbol{f}}{\partial \dot{\boldsymbol{x}}}\dot{\boldsymbol{H}}_S^T\right)dt\ ;\ \hat{\boldsymbol{C}} = \frac{\omega}{\pi}\int_0^{2\pi/\omega} \boldsymbol{H}_S^* \frac{\partial \boldsymbol{f}}{\partial \dot{\boldsymbol{x}}}\boldsymbol{H}_S^T dt \qquad (11)$$

where matrix $\boldsymbol{H}_S^*$ used in the harmonic balance procedure differs from $\boldsymbol{H}_S$ only by a multiplier 0.5 for the components corresponding to zero harmonic (see Ref.[2]). Matrices $\boldsymbol{E}_1$ and $\boldsymbol{E}_2$ are dependent only on the principal vibration frequency:

$$\boldsymbol{E}_1 = diag\left(\boldsymbol{0}, \tilde{\omega}_1^s \begin{bmatrix} \boldsymbol{0} & \boldsymbol{I} \\ -\boldsymbol{I} & \boldsymbol{0} \end{bmatrix}, ..., \tilde{\omega}_{n_s}^s \begin{bmatrix} \boldsymbol{0} & \boldsymbol{I} \\ -\boldsymbol{I} & \boldsymbol{0} \end{bmatrix}\right) \qquad (12)$$

$$\boldsymbol{E}_2 = diag\left(\boldsymbol{0}, \left(\tilde{\omega}_1^s\right)^2 \boldsymbol{I}, \left(\tilde{\omega}_1^s\right)^2 \boldsymbol{I}, ..., \left(\tilde{\omega}_{n_s}^s\right)^2 \boldsymbol{I}\right) \qquad (13)$$

Two types of linear damping can be modelled: (i) viscous damping and (ii) frequency-independent, structural damping and the matrix of linear damping, $\tilde{\boldsymbol{C}}$, takes the form:

viscous damping: $\tilde{\boldsymbol{C}} = \tilde{\boldsymbol{\Xi}}\tilde{\boldsymbol{\Omega}}$; structural damping: $\tilde{\boldsymbol{C}} = \omega^{-1}\tilde{\boldsymbol{\Xi}}\tilde{\boldsymbol{\Omega}}^2$ (14)

where $\tilde{\boldsymbol{\Xi}} = diag(\boldsymbol{\Xi}, \boldsymbol{\Xi}, ...\boldsymbol{\Xi})$; $\boldsymbol{\Xi} = diag\left(\eta_1, \eta_2, ..., \eta_m\right)$ is matrix of prescribed modal damping values.

It should be noted that neglecting the terms in the stability equation which describe the dependency of the nonlinear forces on the acceleration (as was done for a general case in Ref.[12]) does not invoke any loss of generality. This is done here for two reasons: (i) to shorten the formulae and represent the major features of the new method briefly and (ii) taking into account that such dependence of the contact forces on the acceleration is rare in gas-turbine structures.

Now, combining Eqs.(5) and (7) we can write the nonlinear equation for the calculation of the stability boundary:

$$\left\{ \begin{array}{c} \boldsymbol{R}\left(\boldsymbol{X}^n, b_1, \boldsymbol{b}_{2-n_p}(\tau)\right) \\ \lambda_{\mathrm{Re}}^{\max}\left(\boldsymbol{X}^n, b_1, \boldsymbol{b}_{2-n_p}(\tau)\right) \end{array} \right\} = \boldsymbol{0} \qquad (15)$$

The solution of this equation is performed using the Newton-Raphson iterations with the solution continuation (see Refs.[2],[18]). Eq.(15) allows calculation, together with the nonlinear forced response, $\boldsymbol{X}^n$, the value of one selected parameter, b_1, while all the other are varied within some range: $\boldsymbol{b}_{2-n_p}(\tau)$, $\tau \in [0,1]$. The parameter, b_1, which is explicitly calculated from Eq.(15), can be chosen arbitrarily from the set of design parameters of interest, i.e. as it is the most convenient for the analysis.

In the further derivation the excitation frequency is chosen as this parameter, which allows us to calculate the vibration amplitudes and vibration frequencies at the stability boundaries as a function of other design parameters. Moreover, because of inevitable uncertainties in the parameters of structures and operating conditions in practical applications, it may be useful to calculate not only the boundary where the nonlinear periodic regime loses its stability but also the boundaries where the maximum real part of the stability factor takes some prescribed negative acceptable value, λ^*, which provides some safety for the chosen vibration regime in the presence of uncertainties. The value of λ^* has a clear physical meaning which follows from it definition in Eq.(2): it gives the maximum (or minimum for the case of its negative value) rate of the exponential growth (or decay) of the perturbed motion. Accordingly, the stability boundary equation can take the following form to provide the required rate of perturbed motion decay:

$$\left\{ \begin{array}{c} \boldsymbol{R}\left(\boldsymbol{X}^n, \omega, \boldsymbol{b}(\tau)\right) \\ \lambda_{\mathrm{Re}}^{\max}\left(\boldsymbol{X}^n, \omega, \boldsymbol{b}(\tau)\right) - \lambda^* \end{array} \right\} = \boldsymbol{0} \qquad (16)$$

The extended Jacobian of this equation, required for the solution search with the parametric continuation, has the form:

$$\boldsymbol{J}_{ext} = \begin{bmatrix} \partial \boldsymbol{R}/\partial \boldsymbol{X}^n & \partial \boldsymbol{R}/\partial \omega & \partial \boldsymbol{R}/\partial \tau \\ \partial \lambda_{\mathrm{Re}}^{\max}/\partial \boldsymbol{X}^n & \partial \lambda_{\mathrm{Re}}^{\max}/\partial \omega & \partial \lambda_{\mathrm{Re}}^{\max}/\partial \tau \end{bmatrix} \qquad (17)$$

In order to ensure the accuracy, high speed of calculations and robustness of the process of solution, we derive the expressions for all components of this extended Jacobian analytically.

Analytical expressions for matrices used in the stability boundary analysis

The analytical calculation of the first row of the extended Jacobian is generally known from the analysis of resonance amplitudes of the nonlinear forced response (see Ref.[19]). They are modified here for the purposes of the multi-parametric continuation analysis and are expressed in the following form:

$$\frac{\partial \boldsymbol{R}}{\partial \boldsymbol{X}^n} = \boldsymbol{I} + \tilde{\boldsymbol{A}}\hat{\boldsymbol{K}}; \quad \frac{\partial \boldsymbol{R}}{\partial \omega} = -\frac{\partial \boldsymbol{X}^l}{\partial \omega} + \frac{\partial \tilde{\boldsymbol{A}}}{\partial \omega}\boldsymbol{F} \qquad (18)$$

$$\frac{\partial \boldsymbol{R}}{\partial \tau} = -\frac{\partial \boldsymbol{X}^l}{\partial \boldsymbol{b}^l}\frac{\partial \boldsymbol{b}^l}{\partial \tau} - \frac{\partial \boldsymbol{X}^l}{\partial \boldsymbol{b}^p}\frac{\partial \boldsymbol{b}^p}{\partial \tau} + \frac{\partial \tilde{\boldsymbol{A}}}{\partial \boldsymbol{b}^l}\frac{\partial \boldsymbol{b}^l}{\partial \tau}\boldsymbol{F} + \tilde{\boldsymbol{A}}\frac{\partial \boldsymbol{F}}{\partial \boldsymbol{b}^c}\frac{\partial \boldsymbol{b}^c}{\partial \tau} \qquad (19)$$

The expressions for the derivatives of the stability factor, $\lambda_{\mathrm{Re}}^{\max}$, has not be obtained before and are explained here in more details.

The procedure of calculation of these derivatives is the following. At first the full quadratic eigenproblem formulated by Eq.(9) is solved for a vector of nonlinear forced response, $\boldsymbol{X}^n$, and vibration frequency, ω, obtained for a current iteration of the iterative Newt-Raphson solution of Eq.(16). Among all its eigenvalues the value with the maximum real part is selected, $\lambda^{\max}$, and then the right, $\boldsymbol{S}_r$, and left, $\boldsymbol{S}_l$, eigenvectors corresponding to this value are determined. The derivatives of $\lambda^{\max}$ are obtained by differentiating Eq. (9) and then multiplying from the left by $\boldsymbol{S}_l^H$, which gives:

$$\left(\lambda^{\max}\right)' = -\boldsymbol{S}_l^H\left[\lambda^{\max}\boldsymbol{B}_1' + \boldsymbol{B}_0'\right]\boldsymbol{S}_r / w \qquad (20)$$

where $w = \boldsymbol{S}_l^H\left[2\lambda^{\max}\boldsymbol{I} + \boldsymbol{B}_1\right]\boldsymbol{S}_r$; the prime indicates a partial derivative with respect to $\boldsymbol{X}^n$, ω, or τ and superscript 'H' indicates the Hermitian conjugate. Now, let us consider the calculation of each of these three derivatives:

Sensitivity of the stability factor to nonlinear response

To facilitate the calculation of this sensitivity vector, before the calculation of the derivative we project the stability eigenvectors in the space of the mode shapes used for the creation of the reduced stability model, i.e.

$$\boldsymbol{V}_r = \tilde{\boldsymbol{\Phi}}\boldsymbol{S}_r; \quad \boldsymbol{V}_l = \tilde{\boldsymbol{\Phi}}\boldsymbol{S}_l \qquad (21)$$

Now taking derivatives of Eq.(10) and remembering that only $\hat{\boldsymbol{C}}$ and $\hat{\boldsymbol{K}}$ are dependent on $\boldsymbol{X}$ we obtain:

$$\frac{\partial \lambda_{\mathrm{Re}}^{\max}}{\partial \boldsymbol{X}^n} = \mathrm{Re}\left(\frac{\lambda}{w}\boldsymbol{V}_l^H\frac{\partial\left(\hat{\boldsymbol{C}}\boldsymbol{V}_r\right)}{\partial \boldsymbol{X}^n} + \frac{1}{w}\boldsymbol{V}_l^H\frac{\partial\left(\hat{\boldsymbol{K}}\boldsymbol{V}_r\right)}{\partial \boldsymbol{X}^n}\right) \qquad (22)$$

It should be noted that: (i) in this equation only $\hat{\boldsymbol{C}}$ and $\hat{\boldsymbol{K}}$ are dependent on the vector of nonlinear forced response, $\boldsymbol{X}^n$, and (ii) the derivatives are calculated for the vectors of products of these matrices by $\boldsymbol{V}_r$, which makes the evaluation of the expression for the vector $\partial\lambda_{\mathrm{Re}}^{\max}/\partial\boldsymbol{X}^n$ more efficient than the differentiating $\hat{\boldsymbol{C}}$ and $\hat{\boldsymbol{K}}$ alone. These derivatives are calculated analytically for each of the nonlinear contact elements (see some examples in Refs.[2],[19] and [20]) and then combined in the matrices for the whole structure.

Sensitivity of the stability factor to vibration frequency

Differentiating Eq.(10) and multiplying the result by left and right stability eigenvectors we obtain:

$$\boldsymbol{S}_l^H \frac{\partial\left(\boldsymbol{B}_0^r \boldsymbol{S}_r\right)}{\partial\omega} = \boldsymbol{S}_l^H \left[\frac{\partial\tilde{\boldsymbol{C}}}{\partial\omega}\boldsymbol{E}_1 + \tilde{\boldsymbol{C}}\frac{\partial\boldsymbol{E}_1}{\partial\omega} - \frac{\partial\boldsymbol{E}_2}{\partial\omega}\right]\boldsymbol{S}_r + \boldsymbol{V}_l^H \frac{\partial\hat{\boldsymbol{K}}}{\partial\omega}\boldsymbol{V}_r \quad (23)$$

$$\boldsymbol{S}_l^H \frac{\partial\boldsymbol{B}_1}{\partial\omega}\boldsymbol{S}_r = \boldsymbol{S}_l^H \left[2\frac{\partial\boldsymbol{E}_1}{\partial\omega} + \frac{\partial\tilde{\boldsymbol{C}}}{\partial\omega}\right]\boldsymbol{S}_r + \boldsymbol{V}_l^H \frac{\partial\hat{\boldsymbol{C}}}{\partial\omega}\boldsymbol{V}_r \quad (24)$$

Combining these derivatives we obtain the required expression:

$$\frac{\partial\lambda_{\mathrm{Re}}^{\max}}{\partial\omega} = \mathrm{Re}\left(\boldsymbol{S}_l^H \left[\left(\tilde{\boldsymbol{C}} + 2\lambda\boldsymbol{I}\right)\frac{\partial\boldsymbol{E}_1}{\partial\omega} + \frac{\partial\tilde{\boldsymbol{C}}}{\partial\omega}\left(\boldsymbol{E}_1 + 2\lambda\boldsymbol{I}\right) - \frac{\partial\boldsymbol{E}_2}{\partial\omega}\right]\frac{\boldsymbol{S}_r}{w}\right) + \mathrm{Re}\left(\boldsymbol{V}_l^H \left[\frac{\partial\hat{\boldsymbol{K}}}{\partial\omega} + \lambda\frac{\partial\hat{\boldsymbol{C}}}{\partial\omega}\right]\frac{\boldsymbol{V}_r}{w}\right) \quad (25)$$

where

$$\frac{\partial\boldsymbol{E}_1}{\partial\omega} = diag\left(\boldsymbol{0}, k_1^s\begin{bmatrix}\boldsymbol{0} & \boldsymbol{I}\\ -\boldsymbol{I} & \boldsymbol{0}\end{bmatrix}, ..., k_{n_s}^s\begin{bmatrix}\boldsymbol{0} & \boldsymbol{I}\\ -\boldsymbol{I} & \boldsymbol{0}\end{bmatrix}\right) \quad (26)$$

$$\partial\boldsymbol{E}_2/\partial\omega = 2\omega diag\left(\boldsymbol{0}, \left(k_1^s\right)^2\boldsymbol{I}, \left(k_1^s\right)^2\boldsymbol{I}, ..., \left(k_{n_s}^s\right)^2\boldsymbol{I}\right) \quad (27)$$

$$\frac{\partial\tilde{\boldsymbol{C}}}{\partial\omega} = \begin{cases}\boldsymbol{0} & \text{for viscous damping}\\ -\omega^{-2}\tilde{\boldsymbol{\Xi}}\tilde{\boldsymbol{\Omega}}^2 & \text{for structural damping}\end{cases} \quad (28)$$

Sensitivity of the stability factor to tracing parameter

For convenience of presentation the rather lengthy expressions the sensitivity of the stability factor to tracing parameters are given separately for cases: (i) when the parameters of linear part of the structure are varied and (ii) when the contact interface parameters are varied

- for a case of varied contact interface parameters:

$$\frac{\partial\lambda_{\mathrm{Re}}^{\max}}{\partial\tau} = \mathrm{Re}\left(\boldsymbol{V}_l^H\left(\lambda\frac{\partial\hat{\boldsymbol{C}}}{\partial\boldsymbol{b}^c}\frac{\partial\boldsymbol{b}^c}{\partial\tau} + \frac{\partial\hat{\boldsymbol{K}}}{\partial\boldsymbol{b}^c}\frac{\partial\boldsymbol{b}^c}{\partial\tau}\right)\frac{\boldsymbol{V}_r}{w}\right) \quad (29)$$

- for a case of varied linear model parameters:

$$\frac{\partial\lambda_{\mathrm{Re}}^{\max}}{\partial\tau} = \mathrm{Re}\left(\boldsymbol{S}_l^H\left[2\tilde{\boldsymbol{\Omega}}\frac{\partial\tilde{\boldsymbol{\Omega}}}{\partial\boldsymbol{b}^l}\frac{\partial\boldsymbol{b}^l}{\partial\tau} + \left(\frac{\partial\tilde{\boldsymbol{C}}}{\partial\boldsymbol{b}^l}\frac{\partial\boldsymbol{b}^l}{\partial\tau}\right)\left(\boldsymbol{E}_1 + \lambda\boldsymbol{I}\right)\right]\frac{\boldsymbol{S}_r}{w}\right) \quad (30)$$

Calculation of the linear model to its parameters is straightforward for some useful cases, e.g. when the parameter of linear model is j-th natural frequency, ω_j, or modal damping factor, η_j, then

$$\partial\tilde{\boldsymbol{\Omega}}/\partial\omega_j = \boldsymbol{I}_j \quad \text{and} \quad \partial\tilde{\boldsymbol{\Omega}}/\partial\eta_j = \boldsymbol{0} \quad (31)$$

viscous damping	structural damping	
$\partial\tilde{\boldsymbol{C}}/\partial\omega_j = \eta_j\boldsymbol{I}_j$	$\partial\tilde{\boldsymbol{C}}/\partial\omega_j = 2\eta_j\omega_j\omega^{-1}\boldsymbol{I}_j$	(32)
$\partial\tilde{\boldsymbol{C}}/\partial\eta_j = \omega_j\boldsymbol{I}_j;$	$\partial\tilde{\boldsymbol{C}}/\partial\eta_j = \omega_j^2\omega^{-1}\boldsymbol{I}_j$	(33)

where $\boldsymbol{I}_j = diag\left(\boldsymbol{i}_j, ..., \boldsymbol{i}_j\right)$ and $\boldsymbol{i}_j$ is a diagonal matrix with j-th diagonal element equal to 1 while all the other are zeros.

When the sensitivity is required with respect to the design parameters of the structure (e.g. characteristics of geometry or material), the sensitivities of the natural frequencies of the structure with respect to these parameters are determined by differentiating the eigenproblem equation for the linear structure given by:

$$\omega_j' = \phi_j^T\left(\boldsymbol{K}' - \omega_j^2\boldsymbol{M}'\right)\phi_j/\left(2\omega_j\right) \quad (34)$$

The matrix $\partial\tilde{\boldsymbol{\Omega}}/\partial b_j^l$ is then formed from these sensitivities and assuming the proportionality of the damping to the deformation energy, we can write the damping matrix sensitivity for both damping models:

viscous damping	structural damping	
$\boldsymbol{C}' = \eta\tilde{\boldsymbol{\Omega}}';$	$\boldsymbol{C}' = 2\eta\tilde{\boldsymbol{\Omega}}\tilde{\boldsymbol{\Omega}}'$	(35)

Multiparametric analysis of stability boundaries

The method described above allows the calculation of the amplitudes and frequencies at which the system loses it stability under variation of: (i) a single parameter, b_j, or (ii) many parameters which variation is described parametrically: $\boldsymbol{b}(\tau)$. The method can be easily generalised to obtain the dependency of stability loss characteristics when two or several parameters need to be considered as independently varied and, therefore, to obtain the stability domains in the space of these independent parameters. In order to do this we construct a trajectory: $\boldsymbol{b} = \boldsymbol{b}(\tau)$, which have to satisfy the following requirements:

(i) this trajectory has to be continuous together with its derivative with respect to τ - to perform solution continuation;

(ii) the trajectory has to cover the whole domain of possible values: $\boldsymbol{b}^- \le \boldsymbol{b} \le \boldsymbol{b}^+$ more or less uniformly – to describe the parametric dependency over the whole domain without loss of accuracy in some parts of the domain;

(iii) the facility allowing the choice of density for the trajectory coverage over the considered domain should be available - to control the accuracy and computational efforts.

Among possible choices, it was found that the Lissajous curves can be used for such trajectory description. These curves are generalized here for n-dimensional case:

$$b_j = \tfrac{1}{2}\left(b_j^- + b_j^+\right) + \tfrac{1}{2}\left(b_j^+ - b_j^-\right)\sin(l_j\tau + \varphi_j);\ j = 1..n \quad (36)$$

In order to use these functions for the domain sweep a special choice of parameters in Eq.(36) has to be done. The integer numbers, l_j should be different for different parameters, b_j. To have closed trajectories for the variation of parameters the interval of the tracing parameter, τ, providing the closed

trajectories is determined in this case as $[0, 2\pi L]$, where L is the least common multiplier for all l_j in Eq.(36). The larger L the denser is the coverage of the parameter variation domain. Examples of the trajectories are given in Fig. 1 for cases of 2 and 3 varied parameters (with $l_1 = 20$; $l_2 = 18$; $l_3 = 19$ and $\varphi_1 = \pi/2$, $\varphi_2 = \varphi_3 = 0$). The ranges of parameter variation are normalized in this figure to $[-1,1]$, although they can be easily generalized to cover the domain $\boldsymbol{b}^- \le \boldsymbol{b} \le \boldsymbol{b}^+$ (and even domains of more complex shapes).

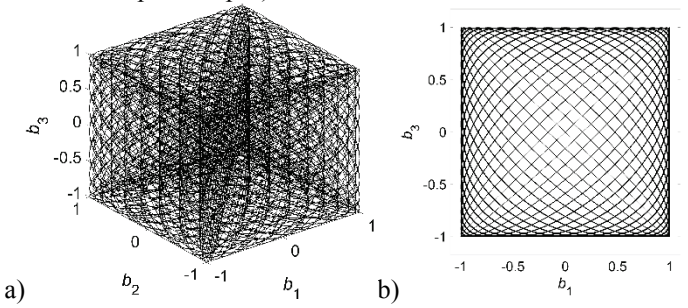

Fig. 1 Examples of the parameter variation trajectories: a) 3D trajectory; b) 2D trajectory

SEARCH OF THE ISOLATED SOLUTION BRANCHES

The very important consequence, which is obtained as a by-product of the developed method for the stability boundary analysis, is the possibility to find the isolated branches of the solutions of the nonlinear forced response equation given by Eqs.(1) and (7). The robustness and efficiency of the method developed in this paper allows the use of the stability tracing as a tool to find isolated solution branches – the problem which does not have a general solution so far. The search of the isolated branches is based on the fact that the stability boundaries in many cases are continuous over the whole manifold of solutions depending on the possible design parameter values. Because of this the trajectory of solutions obtained by solution tracing of Eqs.(15) or (16) provides a solution which go through the stability loss points for all solution branches including the isolated branches.

Some of isolated solution branches are unstable for all points of the solution trajectory, yet they still can be found by the developed method choosing an appropriate value for λ^* in Eq.(16): for this case it can have a positive value in order to find isolated unstable branches. The fully stable closed isolated trajectories do not usually occur in practical systems but a part of the solution trajectory which is fully stable but not connected with the major solution trajectory is a rather usual case and the choice of corresponding negative value for λ^* can help to find new solution trajectories in the domain of design parameter variation which are not connected to the major branch.

NUMERICAL EXAMPLES

The developed method for the parametric analysis of the stability boundaries has been introduced in an in-house FORTRAN computer code ContaDyn developed by the author. The examples of the results of stability boundary analysis for simple models and for a realistic turbine blade model are given below.

A simple model with different nonlinearity types

First example is a one-degree of freedom model described by the following equation:

$$m\ddot{x} + c\dot{x} + kx + f(x) = p\sin\omega t \qquad (37)$$

where $k = 40$; $m = 1$; $c = 0.1/\sqrt{40}$; $p = 100$ and $f(x)$ is the nonlinear force and the cases of nonlinear interaction caused by the following types of the nonlinear interactions are considered here: (i) a cubic nonlinear spring and (ii) a gap nonlinearity. First ten harmonics: from 0 to 9 are used to form multiharmonic nonlinear forced response equations and the same harmonics are used to form the multiharmonic stability equation.

Cubic nonlinear spring. For the cubic spring nonlinearity the nonlinear force function is assumed: $f(x) = k_3 x^3$. The dependency of the maximum forced response on the excitation frequency is shown in **Fig. 2** for different values of the stiffness coefficient: $k_3 = 0.02$; 1; 10 and 100.

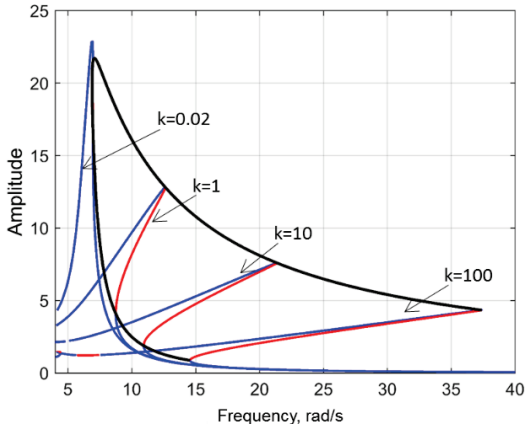

Fig. 2 Forced response and the stability boundary: a case of 1DOF system with cubic nonlinearity

Together with the calculation of the forced response the stability factors are calculated using method provided in Ref.[12] and parts of the solution curves corresponding to stable solution are shown here and further in this paper by blue lines while the unstable solution are drawn by red lines. The black line gives the trajectory of points where the stability changes – which is calculated by the new method. The dependency of the vibration amplitude and frequency at a stability loss boundary as a function of the stiffness coefficient is plotted in **Fig. 3**.

In order to start the process of tracing the stability loss boundary the frequency and the nonlinear multiharmonic amplitude vector are selected at the point on the solution curve where the stability factor changes its sign and this data is used as an initial approximation for the stability boundary calculation. For the considered here case the starting point of the stability boundary curve is chosen at 14.7 rad/s, where the stability loss is detected during calculation of the solution corresponding to $k_3 = 100$ at lower amplitude level. In the process of tracing the stability loss the range of variation of the stiffness coefficient

was set from 100 to 0. With the decrease of the stiffness coefficient the length of the unstable part of the solution trajectory decreases and completely diminishes at approximately $k_3 = 0.02$ - owing to this the process of stability loss tracing turns automatically at the point where the system becomes fully stable and continues to trace the stability loss at higher amplitudes. As a result the whole stability boundary curve is obtained in a single calculation.

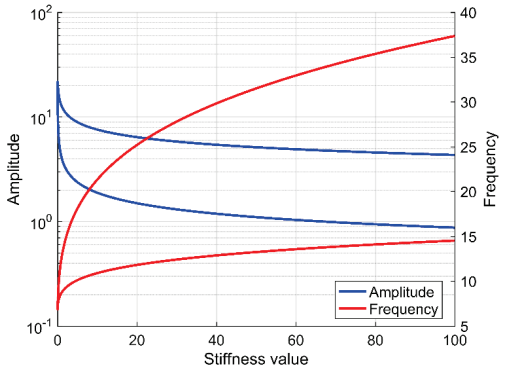

Fig. 3 The amplitude and frequency values at stability loss as a function of cubic stiffness

Gap nonlinearity. For the gap nonlinearity the nonlinear force function is assumed to be $f(x) = k_{gap}x$ for $x >= g$ and $f(x) = 0$ for $x < g$. The forced response amplitudes are shown in **Fig. 4** for different values of the gap stiffness indicated in the figure and the gap value, $g = 10$. The black curve shows the result of parametric analysis of the stability loss, and, again, this curve is calculated in a single calculation.

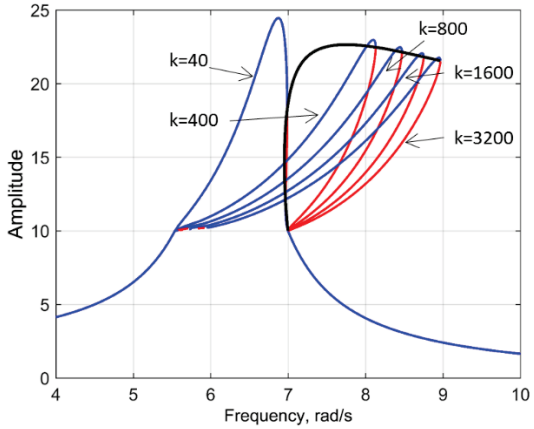

Fig. 4 Forced response and the stability boundary: variation of gap stiffness for 1DOF system

The stability loss amplitude and frequency dependency on the gap stiffness is displayed in **Fig. 5**. One can see that amplitude levels of both points of the stability loss on the solution trajectory (for high and low amplitudes) and the low amplitude frequency are not significantly affected by the gap stiffness variation, while the frequency of high amplitude stability loss changes noticeably.

The effect of variation of gap values on forced response amplitudes is demonstrated in **Fig. 6** for different values of the gap values (gap stiffness is chosen for this case, $k_{gap} = 400$).

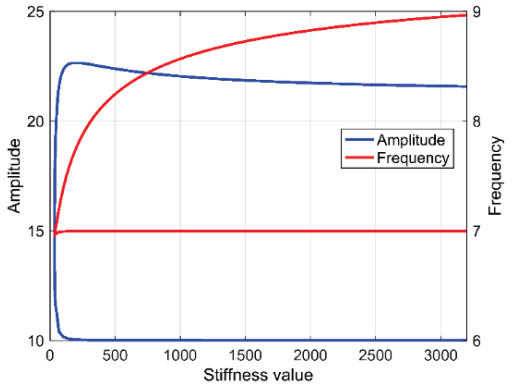

Fig. 5 The amplitude and frequency values at stability loss as a function of gap stiffness value

In this figure in addition to the stability boundary corresponding to $\lambda^* = 0$ (see Eq.(16)) two additional stability boundary curves are plotted: for $\lambda^* = -0.2$ and for $\lambda^* = +0.2$, i.e. over the whole this boundary the maximum Floquet exponent takes these values. The dependency of the stability loss parameters on the gap value calculated directly using the new method is shown in **Fig. 7** for considered here three values of λ^*.

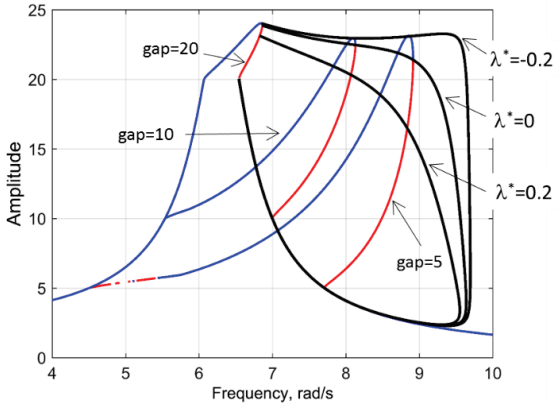

Fig. 6 Forced response and the stability boundary: variation of gap value for 1DOF system

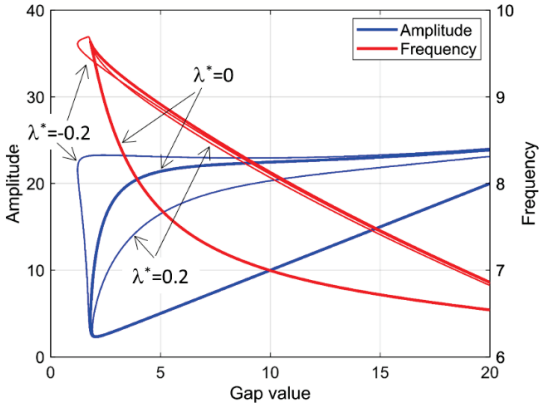

Fig. 7 The amplitude and frequency values at stability loss as a function of gap value

The capability of multi-parametric analysis of the stability boundary is illustrated in **Fig. 8**, where the stability loss amplitude and frequency are calculated as a function of two parameters: gap and stiffness.

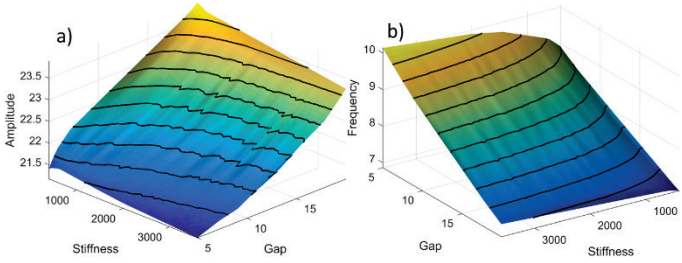

Fig. 8 The amplitude (a) and frequency (b) values at stability loss as a function two contact interface parameters

The parameters are varied along a trajectory shown in **Fig. 1**b and the obtained stability loss amplitude and frequency allow plotting in **Fig. 8** the stability loss surfaces. Some 'waviness' of contour lines observed in **Fig. 8**a occurs due to shortcoming of the available plotting software for cases when the reference points are irregularly distributed over the parameter variation domain: since these points are provided as a result of the solution tracing along the generated trajectory given by Eq.(36) with the variable step size.

A cantilever beam

Another model analysed is a cantilever beam with sides 1000×200×100mm and with the following material properties: elasticity modulus E=10^{5}N/mm^2; density ρ=4.43*10^{-6}kg/mm^3. 2 finite-element beam model is used for the stability sensitivity analysis and the total number of DOFs in the model is 4. The case of viscous damping is considered – to be able to compare the results with some time-domain integration results. The modal damping factors of the beam are 0.02 for all mode shapes. The nonlinear contact interface interaction applied at free end of the beam is considered. The excitation force is applied also at the free end of the beam and the amplitude of the excitation force is 100N. The stability and forced response multiharmonic equations use first 10 harmonics: from 0 to 9.

Cubic nonlinear spring. The stiffness coefficient is varied for the cubic spring example from $k_3 = 10^7$ to $k_3 = 10^3$ N/mm^3. The comparison of the stability boundary calculation with the stability estimates obtained for a set of different stiffness values is shown in **Fig. 9**.

The dependency of the vibration amplitude and frequency at a stability loss boundary as a function of stiffness coefficient is plotted in **Fig. 10**. Comparing the last figure with the results obtained in **Fig. 3** for 1DOF system one can see noticeable differences: for stability loss amplitude and for stability loss frequency.

Gap nonlinearity. The gap nonlinearity produces much more complex and interesting effects for the multi-degree-of-freedom system, as the considered beam is, comparing to the case of 1DOF system. In **Fig. 11** the forced response of a beam with the gap nonlinear parameters $k_{gap} = 10^5$ and $g = 0.1$ is shown.

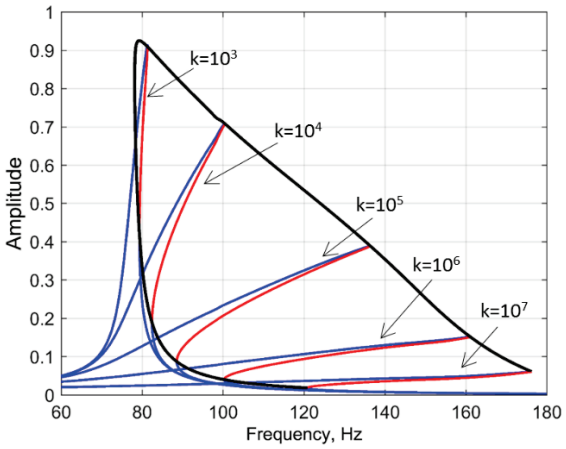

Fig. 9 Forced response and the stability boundary: a case of beam with cubic nonlinearity

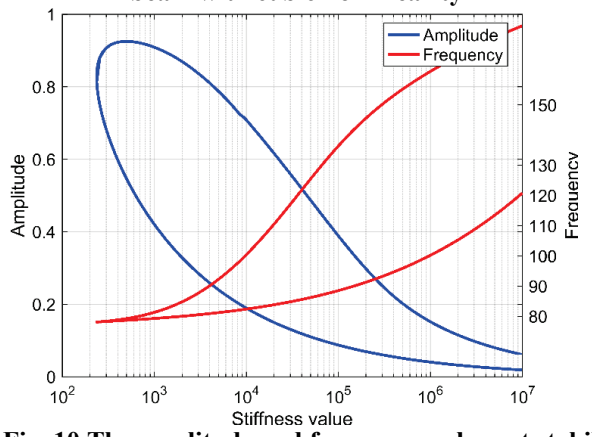

Fig. 10 The amplitude and frequency values at stability loss as a function of cubic stiffness

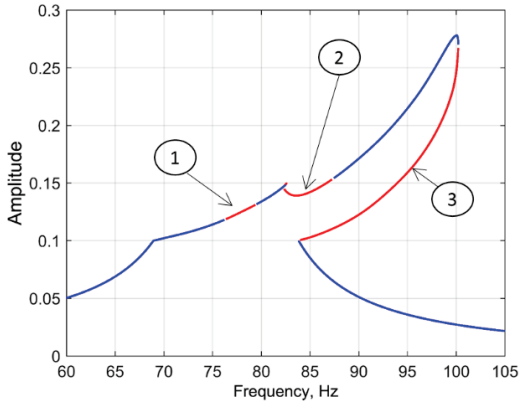

Fig. 11 The forced response amplitude for a beam with gap nonlinearity: $k_{gap} = 10^5$ and $g = 0.1$

It is evident the existence of three unstable parts on the solution trajectory, which are marked by numbers 1, 2 and 3. The unstable part 3 is well known and similar to what can be observed for the case of 1DOF system in **Fig. 4**, but the unstable segments 1 and 2 have not been reported before and require a special analysis.

To understand the stability loss scenarios, for all three cases occurring here, the Floquet multipliers have been calculated for all points on the solution trajectory. The trajectories of the obtained Floquet multipliers are shown in **Fig. 12**. The considered beam model has 4 DOFs and, therefore, it has 8 Floquet multipliers. These multipliers are complex conjugate pairs, for most of the points, and in the figure these pairs of Floquet multipliers are plotted by the same colour.

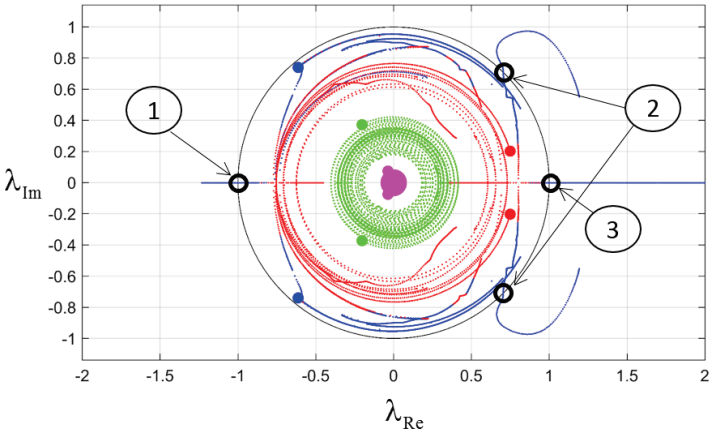

Fig. 12 The trajectories of all Floquet multipliers for the whole range of the excitation frequency variation

When any of the Floquet multipliers leaves the unit circle (plotted also in this figure by a thin black line) the system loses stability. The points where the Floquet multipliers leave the unit circles are shown here by small black circles and the numbers marking these points correspond to the numbers of unstable segments in **Fig. 11**. It is evident that the loss of stability for the segment 1 is performed through a point (-1, 0) which is the well-known indicator of the period-doubling stability loss: i.e. through occurring of the process with a period which is two times larger than the original vibration period. The stability loss of segment 2 is performed through a crossing the unit circle at a point where the Floquet multiplier has imaginary and real parts not equal to zero. This indicates the loss of stability of the periodic motion into quasi-periodic motion. The segment 3 loses its stability through point (+1, 0) – which corresponds to the stability loss of the periodic solution without change of the period value.

In order to check how the system behaves in the conditions close to realistic the nonlinear equations of motion are integrated over time with the varying excitation frequency. The rate of excitation frequency variation is chosen for this case positive (i.e. the excitation frequency increases with the time) and slow enough to obtain the response close to the steady-state periodic vibrations. The results of this analysis are shown in **Fig. 13**, where the blue lines represents the results of time integration.

Because of the very large number of vibration cycles the integrated vibration cycles are merged here in the blue area. The bold red line shows here the results of the multiharmonic frequency domain calculation. The numbered arrows point to the unstable segments indicated above on the forced response curve (see **Fig. 11**). The frequency domain analysis provides a perfect envelope for the time-domain results in all segments where there are stable solutions and on the unstable segments we can observe divergence, since the unstable periodic regimes are not realised in usual conditions.

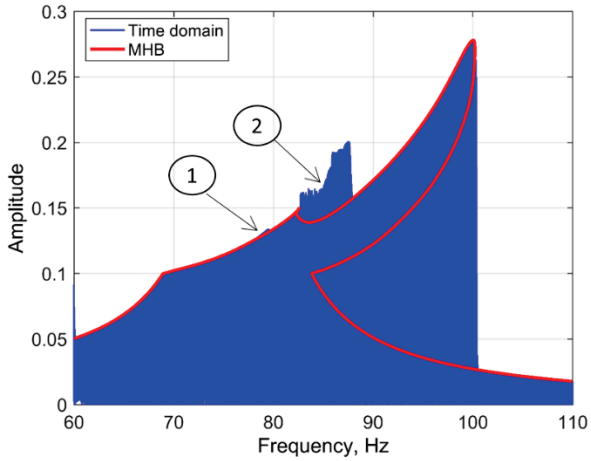

Fig. 13. Forced responses obtained by the time-domain integration and by the multiharmonic balance method

The comparison of the new method for the parametric analysis of the stability loss with the results of stability analysis performed for a chosen set of gap values is shown in **Fig. 14**.

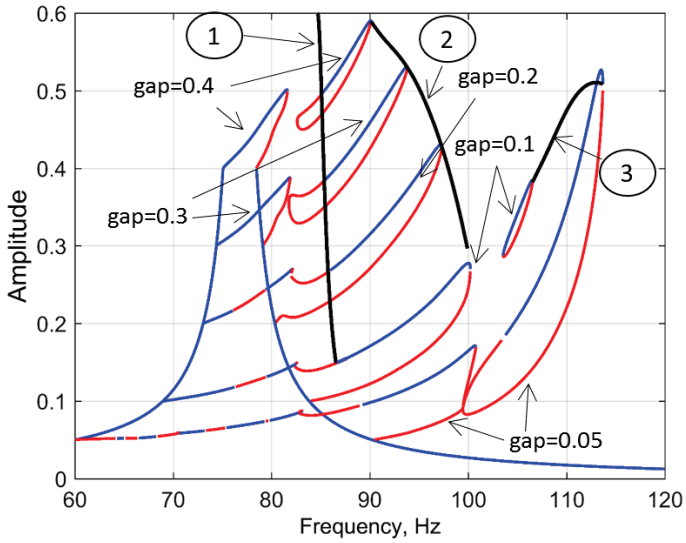

Fig. 14 Forced response and the parametric stability boundary analysis: variation of gap value

The gap stiffness value, $k_{gap} = 10^5$ and the gap values are chosen from 0.05 to 0.4 for the set of systems used for forced response calculations. As before, the black line shows the trajectories of the stability loss points with continuous variation of the gap values. There are three such found trajectories which are marked by numbers in circles. This figure illustrates not only the accuracy of the stability loss boundary calculations but also the capability of using this method for the search of the isolated solution branches. Initially, for each of the selected 5 different gap values the calculation of forced response provided only the

major solution branches. Then the stability loss boundaries were calculated which led to the area in the figure where there were no solutions detected yet. Then, using the solutions found by the new method as initial points at the trajectory searched for, the isolated branches were calculated for gap values; 0.05, 0.1, 0.3, 0.4 – as marked in the figure.

In order to confirm the possibility of the structure to follow the solution belonging to the isolated branch the time integration was performed for the beam with gap value 0.05. The initial conditions for the integration process were chosen from the frequency-domain solution belonging to the isolated branch. The results of the calculation is compared with the frequency-domain analysis in **Fig. 15**. For this case, the excitation frequency was set to decrease with the time.

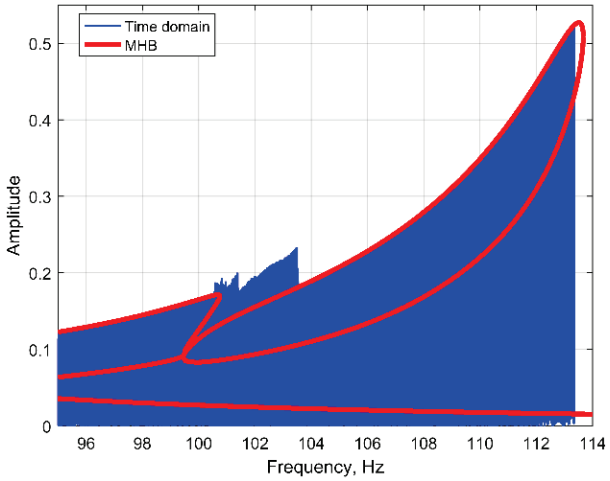

Fig. 15. Time integration and MHB method for the isolated solution branch, gap=0.05

We can observe that the frequency domain solution provides again an envelope for the time-domain solution for segments where the solution is stable. In frequency range 100.8…103.4Hz, where the solution is unstable, the time domain solution is not periodic and its amplitude is irregular, for frequencies lower than 100.8Hz the time domain solution becomes again periodic – because it jumps to the stable solution segment of the major solution branch (as seen in **Fig. 14** for beam with gap=0.05). The possibility of jumping of the vibration regime from an isolated solution branch and to it from the major solution branch during engine deceleration and acceleration highlights the practical importance of the detection of the isolated branches. For the considered here example the amplitude at the resonance peak of the major solution branch is 0.18 but when it jumps to the isolated branch the amplitude can reach value 0.53 – and this high amplitude level would not have be found if we rely only on the solution belonging to the major solution branch.

The example of variation of the amplitude level and vibration frequency at the stability loss point is shown in **Fig. 16** for one of the found stability loss trajectory (marked by number 1 in **Fig. 14**). For the considered range of the gap variation the dependency of the amplitude on the gap is almost linear.

The effect of variation of gap stiffness value on the stability is shown in **Fig. 17**. One can see that the trajectory of the stability loss is calculated by the new method very accurately and, moreover, the tracing of the stability loss boundary allows the detection of the isolated solution branch for the case $k_{gap} = 10^5$. From this figure we can see also the evolution of the shape of the major solution branches when the stiffness changes from 10^3 to 10^5. For the case of $k_{gap} = 3 \cdot 10^4$ the major solution curve is close to forming the isolated solution branch. The sharp reduction of the resonance peak amplitude for the case $k_{gap} = 15 \cdot 10^3$ could be easily overlooked, if the method for tracing the stability boundary was not applied here.

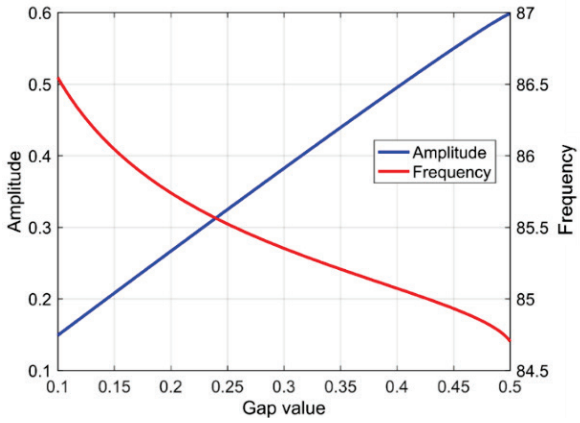

Fig. 16 The amplitude and frequency values at stability loss as a function of gap value

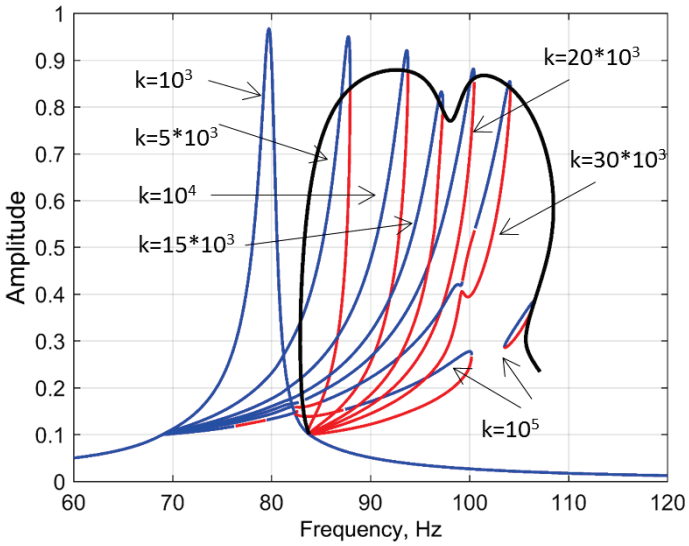

Fig. 17 Forced response and the parametric stability boundary analysis: variation of gap stiffness

The dependencies of the amplitude and frequency at the stability loss on the gap stiffness value as it was traced by the new method is shown in **Fig. 18**.

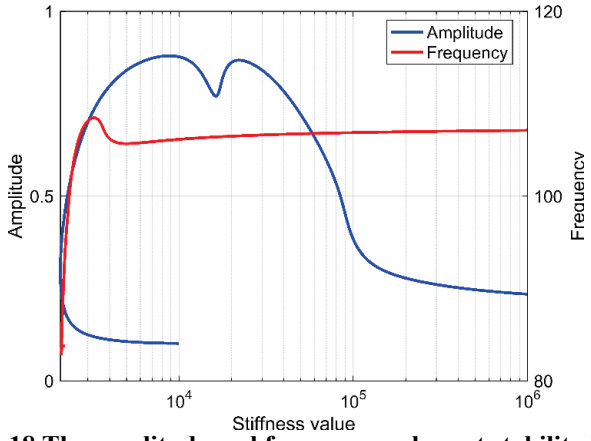

Fig. 18 The amplitude and frequency values at stability loss as a function of gap stiffness

A turbine blade

For the example of application of the developed stability loss boundary tracing method to a system with large number of DOFs, a turbine blade comprising 160,000 DOFs is considered. The blade finite element model is shown in **Fig. 19**.

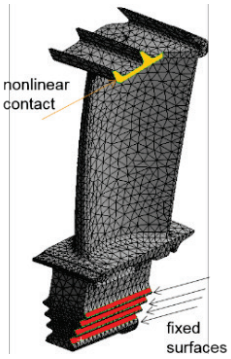

Fig. 19. A cooled turbine blade: a finite element model

The blade is fixed at the blade root contact patches (marked in red in the figure) and the excitation forces are distributed over blade airfoil. The damping is chosen to be structural frequency-independent with all modal damping factors equal to 0.02. 22 cubic nonlinear spring elements are distributed over a contact patch of the blade shroud (marked in yellow in the figure). In the multiharmonic forced response analysis odd harmonics from 0 to 9 are used and in the reduced stability model 8 first blade modes are used.

The trajectory of stability loss points under variation of the stiffness for all 20 cubic nonlinear contact elements is shown in **Fig. 20** together with the results of forced response analyses performed for a set of different values (shown in the figure) of the cubic stiffness. In order to show the details of rather small isolated branches corresponding to stiffness values $k = 3.45*10^8$ and $k = 3.15*10^8$ two zoomed subplots are displayed here also. One can see that the tracing method efficiently finds all stability loss points under continuous stiffness value variation. For this structure the isolated solution branches are found for the case of cubic nonlinearity – which were not detected for considered above simpler models. The isolated branch with $k = 3.45*10^8$ is the isolated branch corresponding to the smallest stiffness coefficient value which contains a stable segment: the stable segment is very small and hardly seen in the figure. This solution branch was found from the stability boundary tracing with $\lambda^* = 0$. In order to find the fully unstable isolated branches the stability boundary tracing has been performed with $\lambda^* = 160$ (the magnitude of λ^* was chosen from the analysis of stability results obtained for the forced response calculated for $k = 5*10^9$). A point corresponding to the smallest stiffness coefficient on this stability boundary (with the offset $\lambda^* = 160$) has been selected and the solution corresponding to this point was used as an initial point on the trajectory of the isolated branch with $k = 3.15*10^8$ to determine the whole isolated branch. This isolated branch is very small and close to collapsing to a point. The isolated branches have not been found for smaller stiffness coefficient values, which can be attributed to the fact that the system becomes too weakly nonlinear for small cubic stiffness coefficient values to exhibit such vibration regimes.

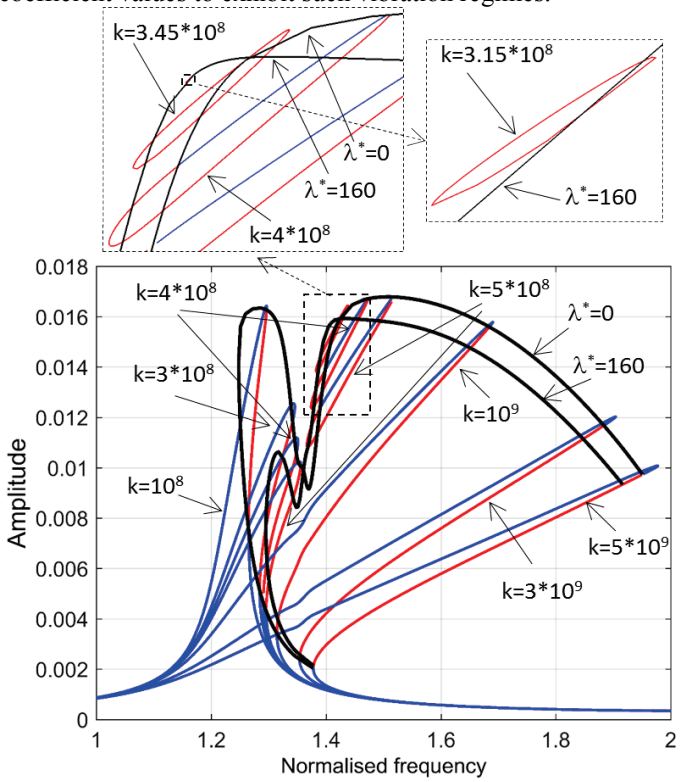

Fig. 20 Forced response and the stability boundary analysis: the variation of cubic stiffness for turbine blade

Here again, the stability boundary tracing method finds stable high amplitude solutions which could be overlooked. For example, the analysis of the major solution branches shows here that the peak amplitude decreases by 60% when the spring stiffness increases from 10^8 to $5•10^8$ yet, if we consider the found isolated branches, we can see that the maximum amplitude value is increased by 5% instead of the decrease.

The dependencies of the amplitude and frequency at the stability loss on the stiffness value for the turbine blade is shown in **Fig. 21**, where the complex character of these dependencies can be observed which can be captured accurately by the proposed method.

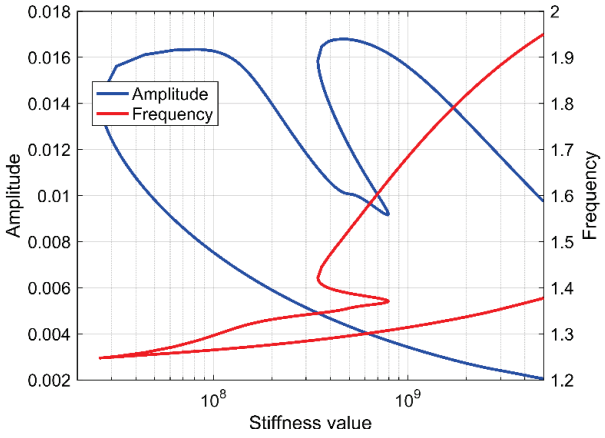

Fig. 21 The amplitude and frequency values at stability loss as a function of cubic stiffness for turbine blade

The behaviour of all the stability factors during the stability loss solution tracing is demonstrated in **Fig. 22**. Since the reduced stability models uses 8 modes shape the total number of stability factors calculated is 16, and the real parts of these, generally complex numbers determine the vibration regime stability. The stability factors are calculated for each step of the stability boundary tracing and for each such step the stability factors are plotted by dots of different colours. The step size over the stiffness value is varied during the solution tracing process. It is chosen by the code automatically to provide the fast convergence of the Newton-Raphson iterations.

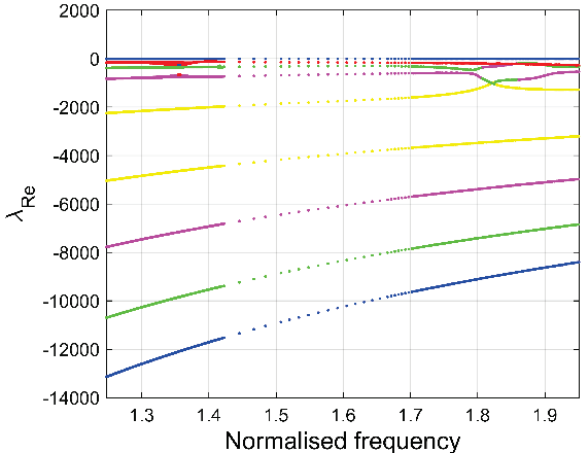

Fig. 22 Variation of all stability factors along the stability loss solution trajectory

Depending on the step size, the dots corresponding to stability factors look in the plot as merged for some ranges of vibration frequency - where the steps are small and for the frequency range [1.43, 1.66] they are separated dots - where the steps are sufficiently large. Some of the 16 stability factor plots are overlapped on some parts of their trajectories. We can observe that the maximum value of the real parts is 0, as it should be, and the stability factors vary rather gradually and smoothly with the variation of the vibration frequency.

The numerical efficiency of the proposed method and computer code is illustrated in Table 1, where times spent for the calculation of three major analysis types for the cooled turbine blade considered here are shown: (i) the calculation of nonlinear forced response without the stability analysis; (ii) the calculation of the nonlinear forced response together with the determination of the stability factors; and (iii) the stability boundary analysis using the proposed method. From the considered here cases the examples of the forced response calculated for the stiffness coefficient value $k=10^9$ are given. It should be noted that the first implementation of the stability boundary analysis in the FORTRAN code was focused on the exploring of the new method capabilities rather than on the numerical efficiency of the computations and its computation speed has a good potential to be increased further. The calculations were performed on a laptop with two-core Intel 1.7 GHz processor. Owing to the fact that the computer code is well-parallelized the wall time is smaller than the total CPU time spent by both processors approximately by factor of 2.

Table 1. The examples of the computational time

Type of the analysis	Total CPU time	Wall time
Forced response without stability analysis ($k=10^9$)	77 sec	46 sec
Forced response with stability analysis ($k=10^9$)	390 sec	200 sec
Stability boundary analysis	8576 sec	4305 sec

CONCLUSIONS

A method for parametric analysis of the stability loss boundary has been developed for a first time.

The method allows the calculation in frequency domain, for periodic regimes of nonlinear forced vibrations, the stability loss points together with the vibration amplitudes and design parameter values corresponding to the stability boundaries. The tracing algorithm is applied to obtain the trajectories of stability loss points as functions of design parameters.

The parametric stability loss is formulated for cases when: (i) the design parameters characterise the properties of nonlinear contact interfaces (e.g. gap, contact stiffness, friction coefficient, etc.) and (ii) the design parameters describe linear components of the analysed structure (e.g. parameters of geometric shape, material, natural frequencies, modal damping etc.) and (iii) these parameters describe the excitation loads (e.g. their level, distribution or frequency). An approach allowing the multiparametric analysis of stability boundaries is proposed.

The method uses the multiharmonic representation of the periodic forced response and aimed at the analysis of realistic

gas-turbine structures comprising thousands and millions degrees of freedom.

The method can be used for the effective search of isolated branches of the nonlinear solutions and examples of detection and search of the isolated branches are given: for relatively small and for large-scale finite element models.

The efficiency of the method is demonstrated on simple systems and on a large-scale model of a turbine blade.

REFERENCES

[1] Cardona, A., Coune, T., Lerusse, A., and Geradin, M., (1994) "A multiharmonic method for nonlinear vibration analysis", *Int. J. for Num. Meth. in Eng.,* Vol. 37, No. 9, pp. 1593-1608

[2] Petrov, E.P., Ewins, D.J., 2003, "Analytical formulation of friction interface elements for analysis of nonlinear multi-harmonic vibrations of bladed discs", *ASME J. of Turbomachinery*, Vol.125, pp.364-371

[3] Petrov,E.P., (2011) "A high-accuracy model reduction for analysis of nonlinear vibrations in structures with contact interfaces", *Trans. ASME J. Eng. Gas Turbines and Power*, Vol. 133(10), 102503

[4] Zucca, S., C.M. Firrone, and M.M. Gola, (2012). Numerical assessment of friction damping at turbine blade root joints by simultaneous calculation of the static and dynamic contact loads. *Nonlinear Dynamics*, 67(3): p. 1943-1955.

[5] Krack, M., Panning-von Scheidt, L., Wallaschek, J. (2017). "On the Interaction of Multiple Traveling Wave Modes in the Flutter Vibrations of Friction-Damped Tuned Bladed Disks." *J. of Eng. for Gas Turbines and Power*, 139(4), 042501

[6] Batailly, A., Legrand, M. et al. (2012). "Numerical-experimental comparison in the simulation of rotor/stator interaction through blade-tip/abradable coating contact." *J. of Eng. for Gas Turbines and Power*, 134(8).

[7] Lewandowski, R. (1997). "Computational formulation for periodic vibration of geometrically nonlinear structures. Part 1. Theoretical background." Int. J. of Solids and Structures 34(15): 1925-1947

[8] Von Groll, G. and Ewins, D.J. (2001) "The harmonic balance method with arc-length continuation in rotor/stator contact problems", *J. of Sound and Vibration*, v 241, n 2, p 223-233

[9] Villa, C., J.-J. Sinou, and F. Thouverez (2008). "Stability and vibration analysis of a complex flexible rotor bearing system." Communications in Nonlinear Science and Numerical Simulation 13(4): 804-821.

[10] Lazarus, A. and O. Thomas (2010). "A harmonic-based method for computing the stability of periodic solutions of dynamical systems." Comptes Rendus Mecanique 338(9), pp. 510-517.

[11] T. Detroux, L. Renson, L. Masset, G. Kerschen (2015). The harmonic balance method for bifurcation analysis of large-scale nonlinear mechanical systems", Comput. Methods Appl. Mech. Engrg. 296 (2015) 18–38

[12] E. Petrov, (2017) "Stability analysis of multiharmonic nonlinear vibrations for large models of gas-turbine engine structures with friction and gaps", *Trans. ASME: J. Eng. Gas Turbines and Power*, Vol. 139, pp.022508/1-102502/10

[13] E. Petrov, (2018) "Frequency-domain sensitivity analysis of stability of nonlinear vibrations for high-fidelity models of jointed structures", *Trans. ASME J. Eng. Gas Turbines Power,* 140(1), 012508; doi: 10.1115/1.4037708

[14] Duan, C., and Singh, R., 2008. "Isolated sub-harmonic resonance branch in the frequency response of an oscillator with slight asymmetry in the clearance". J. of Sound and Vibration, 314, pp. 12–18

[15] J.Noël, T.Detroux, L.Masset, G.Kerschen, L.Virgin, Isolated response curves in a base-excited two-degree-of-freedom, nonlinear system, Proc. ASME 2015 Int. Design Eng. Tech. Conf., IDETC/CIE 2015, Boston, USA

[16] Grolet, A., Thouverez, F., (2015). Computing multiple periodic solutions of nonlinear vibration problems using the harmonic balance method and Groebner bases, *Mechanical Systems and Signal Processing*, Vol.52–53, pp. 529-547

[17] Hill, T., Neild, S, and Cammarano, A., (2016). "An analytical approach for detecting isolated periodic solution branches in weakly nonlinear structures". J. of Sound and Vibration, 379, pp. 150–165.

[18] Fried, I., (1984). "Orthogonal Trajectory Accession to the Nonlinear Equilibrium Curve", Comput. Methods Appl. Mech. Eng., 47, pp. 283–297.

[19] Petrov, E.P., (2007), "Direct parametric analysis of resonance regimes for nonlinear vibrations of bladed discs", Trans. ASME: J. of Turbomachinery, Vol.129, pp.495-502

[20] Petrov, E.P., (2005), "Sensitivity Analysis of Nonlinear Forced Response for Bladed Discs with Friction Contact Interfaces", Proc. of ASME Turbo Expo, June 6–9, 2005, Reno-Tahoe, USA, GT2005-68935